Digest Journal of Nanomaterials and Biostructures Vol. 8, No. 1, January - March 2013, p. 433 - 444

NOVEL UREIDO-4'-AMINOBENZO-15-CROWN-5-ETHER PERIODIC MESOPOROUS SILICAS

E. VASILE, F. DUMITRU[a*], A. RAZVAN[a], O. OPREA[a], C. ANDRONESCU[b]
METAV Research and Development, 31 C.A. Rosetti, sector 2, Bucharest, Romania
[a]*Politehnica University Bucharest, Department of Physical and Inorganic Chemistry and Electrochemistry , 1 Polizu st., 011061, Bucharest, Romania,*
[b]*Politehnica University Bucharest, Department of Polymer Science, 149 Calea Victoriei, 010072, Bucharest, Romania*

We have prepared ordered mesoporous silicas incorporating the ureido benzo-crown ether: 3-(triethoxysilyl) propyl isocyanate modified 4'-aminobenzo-15-crown-5 ether, TESPIC-CE, either by direct synthesis (co-condensation method, *route A*) or by post-synthesis grafting strategy (*route B*). Elemental analysis and XPS measurements, FT-IR spectra, TG/DSC analyses, X-ray powder diffraction, TEM/HRTEM, and N_2 sorption isotherms were used to characterise the novel functionalized mesoporous silicas. Grafting of ureido benzo-crown ether onto silica inner surface resulted in the reduction of surface area from ~1000 m^2/g of the pure MCM-41 used as reference to 707 m^2/g for MCM-$41_{B(TESPIC-CE)}$ and to 903 m^2/g for MCM-$41_{B(TESPIC)+CE}$, suggesting that for comparable TESPIC-CE content into silica framework, the heterogeneous method lead to better sorption properties: higher surface area and more efficiently grafting of crown ether inside pores. Interestingly, the MCM-$41_{A(TESPIC-CE)}$ silica obtained by template-directed co-condensation reaction exhibits a relatively high surface area (618 m^2/g) while containing about twice as much organic content into mesoporous framework than MCM-$41_{B(TESPIC-CE)}$ or MCM-$41_{B(TESPIC)+CE}$.

(Received February 5, 2013; Accepted February 18, 2013)

Keywords: Mesoporous silica, Crown ether, Co-condensation, Grafting

1. Introduction

Acknowledging that unexplored functions can be found within the confined spaces of mesopores, many research works have been conducted in order to enhance the potential of mesoporous materials in binding, recognition and selection applications [1]. Multiple molecular recognition features can be transferred in solid material by incorporating, either through co-condensation or through post-synthetic grafting methods, functional ligands on silica surface. As numerous papers have pointed out [2], crown ethers, with their easy tunable molecular recognition properties, are very interesting compounds for the preparation of chemical modified silica affording hybrid materials for selective and advanced separation processes. Since the exhaustive studies of Bradshaw et al. [3] on selective extraction of alkali and alkaline earth metal ions by crown-ether modified silica gel as chemically bonded phase in chromatography, more complex *structure-directed function* crown-ether hybrid materials have been developed: from *heteropolysiloxane fixed-site complexant membrane* [4], which simultaneously transports adenosine triphosphate (ATP^{2-}) anions and sodium cations, to *dynamic constitutional mesoporous materials,* used for mimicking the adaptive structural functionality of natural ion-channel systems [5, 6]. In these *heteropolysiloxane fixed-site*

*Corresponding author f.dumitru@oxy.pub.ro

complexant membranes, the fixed crown ether is not a carrier; it assists and controls the "fixed-site jumping" diffusion of solutes into the dense silica material by the ion-pair recognition between the covalently fixed complexant – a heteroditopic ureido crown-ether – , and Na^+/ATP^{2-} or Cl^- ions [4]. On the other hand in the *dynamic constitutional mesoporous materials* reported by the same group [5, 6], the functional self-organized heteroditopic crown ethers are reversibly connected with the mesoporous silica scaffolding matrix through hydrophobic noncovalent interactions and these materials exhibit an adaptive behavior: they adapt and evolve their internal structure to improve their ion-transport properties toward the fittest ion-channel. These examples demonstrated that, in the endless quest for new materials, material topology changes used to tune the ion selectivity represent a powerful approach. In the same context, Kimura et al. [7] reported ion-sensing membranes incorporating crown ether moiety whose selectivity drastically changes when ordered mesoporous silica is adopted as the scaffold material instead of the conventional sol-gel silica. While the crown ether moieties in conventional sol–gel derived membranes are randomly distributed and they tend to form metal complexes with a 1 : 1 stoichiometry of metal ion and crown ether ring, in ordered mesoporous silica two neighboring crown-ether rings behave like a bis(crown ether) molecule by their cooperative action [bis(crown ether) effect] to form sandwich-type metal complexes with a 1 : 2 stoichiometry. This is the case of 15-crown-5 ether which exhibits Na^+-selectivity when incorporated in a sol–gel derived membrane, while in mesoporous periodic silica exhibits high affinity for K^+ over Na^+ due to the bis(15-crown-5) effect [7].

Toward the objective of developing new hybrid, structure-directed function materials, we have prepared ordered mesoporous silicas incorporating a functionalized 4'-aminobenzo-15-crown-5 ether either by direct synthesis (co-condensation route) or by post-synthesis grafting strategy. The crown ether, **TESPIC-CE**, designed to be grafted into silica solid matrix has molecular recognition sites for the anion (urea moieties) and the cation (macrocyclic cavity, d=1.7-2.2Å) covalently linked, urea linkages also guiding the supramolecular interaction by H-bond association, and easy polymerizable $Si(OEt)_3$ terminal groups as structural features (*Scheme 1*). This heteroditopic crown ether, obtained by condensation of 4'-aminobenzo-15-crown-5 with the silane coupling agent 3-(triethoxysilyl)-propyl isocyanate (TESPIC), has been reported as a constituent of a series of hybrid sol-gel materials such as thermoresponsive polysilsesquioxane-crown ether hybrids [8], ion-channel-type columnar architectures in G-quadruplex-ureidocrown ether constitutional hybrids [9], magnetic nanoparticle (MNP)-supported crown ethers as phase-transfer catalysts [10, 11], self-organized urea-crown ether membrane [12], hybrid nanomaterial functioning as an ion-powered ATP^{2-} pump [4], stationary phases for the chromatographic separation of metal cations [13], but there is no mention about its inclusion in mesoporous silica materials.

Two routes to obtain new crown ether mesoporous silicas have been pursued, one in which **TESPIC-CE** was covalently bonded to the framework of MCM-41 by co-condensation with tetraethoxysilane (TEOS) by using the cetyltrimethylammonium bromide (CTAB) surfactant as template (*Scheme 1, route A*), and the other path which refers to chemically grafting of the 4'-aminobenzo-15-crown-5 ether or **TESPIC-CE** onto MCM-41 by homogeneous and heterogeneous methods (*Scheme 1, route B*).

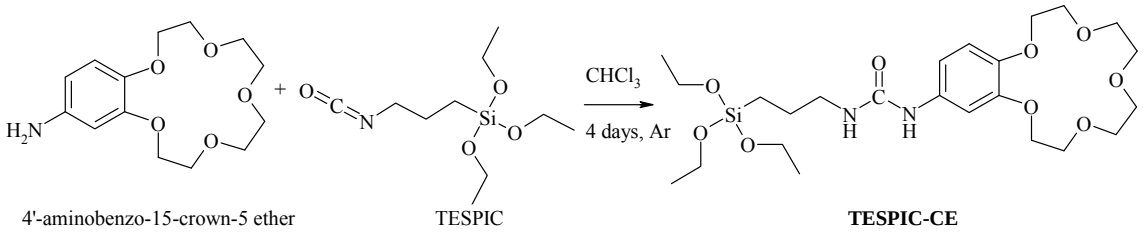

4'-aminobenzo-15-crown-5 ether TESPIC **TESPIC-CE**

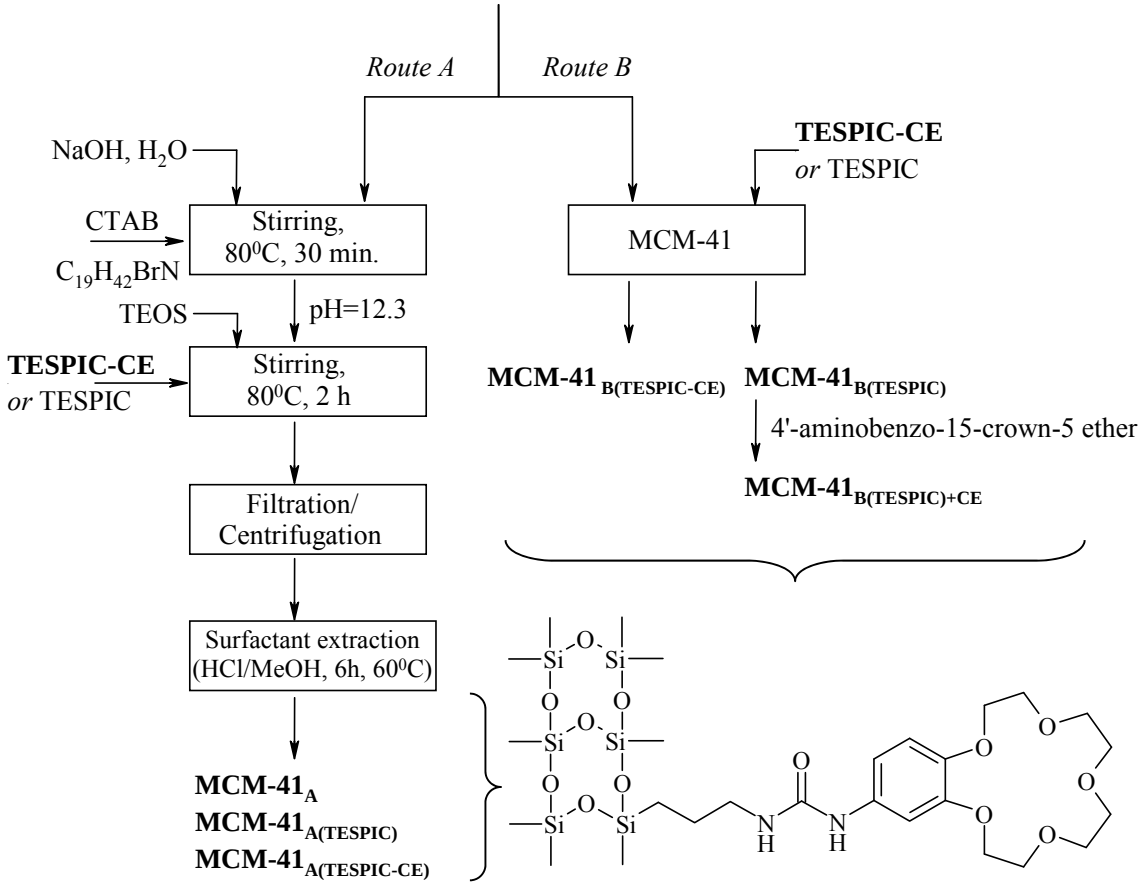

Scheme 1. Preparation of ureido-4'-aminobenzo-15-crown-5-ether mesoporous silicas

Elemental analysis and XPS measurements, FT-IR spectra, TG/DSC analyses, X-ray powder diffraction, TEM/HRTEM, and N_2 sorption isotherms were used to characterise the novel functionalized mesoporous silicas.

2. Experimental

2.1. Techniques and materials

4'-Aminobenzo-15-crown-5 ether 97%, 3-(triethoxysilyl)-propyl isocyanate (TESPIC) 95%, cetyltrimethylammonium bromide (CTAB), were commercially available (Aldrich) and used as received. Tetraethoxysilane (TEOS) was purified by drying over 4Å molecular sieves followed by a vacuum distillation. All the solvents (hexane, chloroform, and toluene) were used after desiccation over molecular sieves (4Å). MCM-41 (silica mesostructured, hexagonal framework, unit cell size ~4.6 nm) used in post-grafting synthesis (*Scheme 1, route B*) was also purchased from Aldrich.

Elemental analyses were carried out on a Heraeus CHNO-Rapid apparatus (Institut für Anorganische Chemie, RWTH Aachen). FT-IR vibrational spectra were recorded with a Bruker Tensor 27 spectrophotometer, with the ATR sampling unit, in the wavenumbers range of 500-4000 cm^{-1}.

Thermal analysis TG-DSC of the compounds was followed with a Netzsch 449C STA Jupiter. Samples were placed in open Pt crucible and heated with $10K \cdot min^{-1}$ from room temperature to 900°C, under the flow of $20mL \cdot min^{-1}$ dried air. An empty Pt crucible was used as reference.

Powder X-ray diffraction (PXRD) patterns were recorded on a Panalytical X`PERT PRO MPD diffractometer with graphite monochromatized CuK_α radiation (λ=1.54 Å). The samples were scanned in the Bragg angle, 2θ range of 2-10º, with a a step size of 0.013º.

TEM and HRTEM images were taken using a TECNAI F30 G^2 high-resolution transmission electron microscope operated at an accelerating voltage of 300-kV device. The sample for TEM/HRTEM imaging was prepared by dispersing a large number of product particles by ultrasonication in methanol by vibrating and then collecting the sample into a holey carbon-coated TEM support grid.

X-ray photoelectron spectroscopy (XPS) data were recorded on a Thermo Scientific K-Alpha equipment, fully integrated, with an aluminium anode monochromatic source. Survey scans (0-1200 eV) were performed to identify constitutive elements.

The specific surface area of mesoporous silicas were measured by BET method with N_2 sorption. The BET measurements were carried out on Gemini V2.00 (GEMINI 2365 Porosimeter Micromeritics Instrument Corp.).

2.2. Synthesis of 4-[3-triethoxysilyl)propyl]ureidobenzo-15-crown-5 ether, TESPIC-CE

First, the ureido benzo-crown **TESPIC-CE** was prepared via the reaction of the terminal amine groups of 4'-aminobenzo-15-crown-5 ether and the isocyanate group of TESPIC with a molar ratio of 1:1 to form the urea linkage. In a typical synthesis, 4'-aminobenzo-15-crown-5 ether (1.76 mmol, 0.5 g) was dissolved in 20 mL of $CHCl_3$ and stirred at 64ºC, under argon atmosphere. TESPIC (1.76 mmol, 0.46 mL) was added to the above solution and continuously stirred for 4 days at 64ºC. After removal of the solvent, the residue was crystallized from n-hexane to afford **TESPIC-CE** as a white powder (yield 85%, 0.8g). The method was adapted from literature [4-6].

^{1}H-NMR ($CDCl_3$, 400 MHz, ppm, δ): 0.590-0.631 (t, 2H, CH_2-Si-), 1.181-1.251 (m, 9H, -CH_3), 1.573-1.649 (q, 2H, -CH_2), 3.195-3.230 (t, 2H, -CH_2-NH-), 3.685-3.747 (m, 10H, -CH_2-O-), 3.766-3.819 (q, 6H, -CH_2-O-), 3.863-3.898 (m, 4H, -CH_2-O-), 4.086-4.096 (m, 4H, -CH_2-O-), 6.669-6.695 (d, 1H, H^{ar}), 6.777-6.798 (d, 1H, H^{ar}), 6.965-6.960 (s_{br}, 1H, H^{ar}).

IR (cm^{-1}): 1668 (NHCO), 1100.09-1072.83 (CH_2-O-Si-).

2.3. Preparation of functionalized mesoporous silica

The second stage was to conduct preparation of mesoporous periodic silica of MCM-41 type with the synthesised crown ether, **TESPIC-CE**, either by co-condensation between **TESPIC-CE** and TEOS (*Scheme 1, Route A*) or by chemical grafting of **TESPIC-CE** onto silica surface (*Scheme 1, Route B*).

Route A (Scheme 1): Mesoporous silicas (Table 1) were prepared by using cetyltrimethylammonium bromide (CTAB), organotrialkoxysilane **TESPIC-CE** or TESPIC and tetraethoxysilane (TEOS) as sol precursors to form silica mesopores. The reaction mixture contained 1.0 CTAB: 8.16 TEOS: 1.05 organotrialkoxysilane precursor (**TESPIC-CE** or TESPIC): 2.55 NaOH: 4857 H_2O as molar ratio [14]. First, the mixture of CTAB and NaOH in water was heated at 80°C for 30 min when the pH 12.3 was reached. At this point, TEOS and organotrialkoxysilane precursor (**TESPIC-CE** or TESPIC) were added. Maintaining the reaction mixture at 80°C for 2 h, then quenched by cooling the solution to the room temperature, white solids (**MCM-41$_{A(TESPIC-CE)}$** and **MCM-41$_{A(TESPIC)}$**) precipitated. The products were isolated by filtration, washed with large volumes of water and methanol and dried in oven at 105°C for 6 h. The surfactant (CTAB) was removed by acid extraction with concentrated HCl (1 mL) in methanol (100 mL) at 60°C for 6 h. Pure **MCM-41$_A$** was prepared as reference using the same experimental conditions.

Route B (Scheme 1): The second methodology involves the chemical modification of commercially available MCM-41 mesoporous silica with crown ether moiety by two conventional methods, the homogeneous and heterogeneous methods.

- Heterogeneous method involves a two step functionalization of the MCM-41 silica: first, the silylating agent, 3-(triethoxysilyl)-propyl isocyanate (TESPIC), reacted with the surface hydroxyl groups to give the isocyanate-functionalized silica, **MCM-41$_{B(TESPIC)}$** (Table 1) and in a second reaction, unmodified 4'-aminobenzo-15-crown-5 ether (CE) was covalently grafted onto **MCM-41$_{B(TESPIC)}$** to afford the **MCM-41$_{B(TESPIC)+CE}$** silica (Table 1).

MCM-41 was derivatized with 3-(triethoxysilyl)-propyl isocyanate by a reaction between MCM-41 (3g, dried at 160°C for 5 h, under vacuum, to remove adsorbed water molecules) and TESPIC (1.3 mL, 5 mmol) in toluene (200 mL). The reaction was run for 24 h under Ar-atmosphere. The resulting **MCM-41$_{B(TESPIC)}$** was collected by centrifugation, then soaked in toluene for 24 h to remove adsorbed TESPIC, filtered and dried under reduced pressure. Refluxing **MCM-41$_{B(TESPIC)}$** (100 mg) in a $CHCl_3$ solution of 4'-aminobenzo-15-crown-5 ether (CE) (0.15 mmol) for 24 h under argon afforded **MCM-41$_{B(TESPIC)+CE}$**.

- In the homogeneous method, the pre-synthesized **TESPIC-CE** (0.08 g, 0.15 mmol) reacted with the silanol groups of activated silica (MCM-41, 100 mg) in $CHCl_3$, 24 h, under argon, thus leading to **MCM-41$_{B\ (TESPIC\text{-}CE)}$** silica (Table 1).

Table 1. Organic content of mesoporous silicas as determined by chemical analysis and XPS

Mesoporous silicas	Found (%wt) (by elemental analysis)			Found (%wt) (by XPS)		
	C	H	N	C	H	N
MCM-41$_{A(TESPIC)}$	7.13	2.3	2.17	7.32	-	2.89
MCM-41$_{A(TESPIC\text{-}CE)}$	13.7	2.93	4.59	11.73	-	6.93
MCM-41$_{B(TESPIC)}$	6.48	0.8	1.19	6.22	-	1.6
MCM-41$_{B(TESPIC)+CE}$	8.23	0.79	1.37	8.65	-	1.95
MCM-41$_{B\ (TESPIC\text{-}CE)}$	6.65	2.04	1.14	5.21	-	1.41

3. Results and discussion

3.1. FT-IR spectra

The presence of the organic moieties (TESPIC or **TESPIC-CE**) covalently bonded to the mesoporous silicas was confirmed by FT-IR absorption spectra. Absorption bands characteristic for the stretching vibrations of isocyanate linkage (~2270 cm^{-1}) in **MCM-41$_{A(TESPIC)}$** and **MCM-41$_{B(TESPIC)}$** or amide bonds (NHC=O, ~1668 cm^{-1}) in **MCM-41$_{A(TESPIC\text{-}CE)}$**, **MCM-41$_{B(TESPIC)+CE}$**, and **MCM-41$_{B(TESPIC\text{-}CE)}$** are good reasons to claim the organo-derivatization of silica. Moreover, as a consequence of hydrolysis/condensation reactions between the silica precursors, the doublet signals assigned to the Si-O-C bonds (1100.09-1072.83 cm^{-1}) in TESPIC or **TESPIC-CE** disappear and instead of them strong and broad signals of Si-O-Si from silica network could be identified at ~1100 cm^{-1} (Fig. 1).

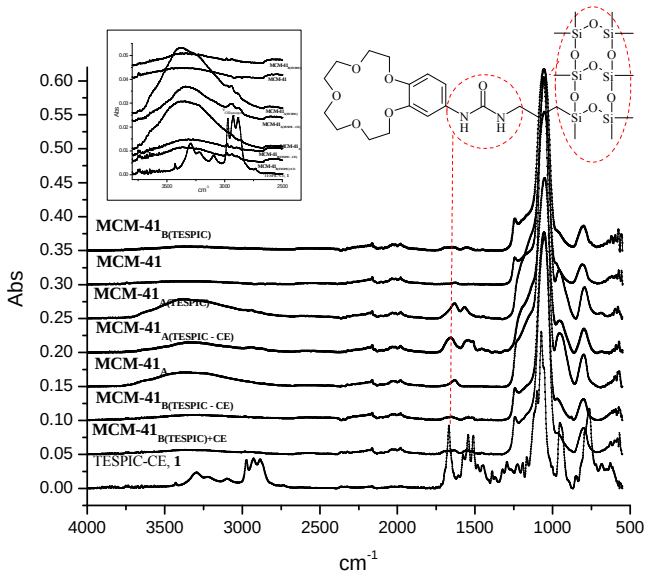

Fig.1. FT-IR spectra of the synthesised mesoporous silica. The inset graph shows the 4000-2500 cm^{-1} region with the alkyl symmetric and asymmetric stretching vibrations.

3.2. Elemental analysis and XPS data

Further arguments on the chemical structure of mesoporous silicas: **MCM-41$_{A(TESPIC)}$**, **MCM-41$_{A(TESPIC-CE)}$**, **MCM-41$_{B(TESPIC)}$**, **MCM-41$_{B(TESPIC)+CE}$**, and **MCM-41$_{B(TESPIC-CE)}$** were obtained by X-ray photoelectron spectroscopy.

From XPS scans (Fig. 2) performed on **MCM-41$_{A(TESPIC)}$** and **MCM-41$_{B(TESPIC)}$** it follows that they have as constitutive elements : C - *C1s (**MCM-41$_{A(TESPIC)}$** - 285.27 eV, **MCM-41$_{B(TESPIC)}$** - 284.97 eV)*, N - *N1s (**MCM-41$_{A(TESPIC)}$** - 400.08 eV, **MCM-41$_{B(TESPIC)}$** – 398.59 eV)*, Si - *Si2p (**MCM-41$_{A(TESPIC)}$** – 103.2 eV, **MCM-41$_{B(TESPIC)}$** – 105.7 eV)*, and O - *O1s (**MCM-41$_{A(TESPIC)}$** - 532.85 eV, **MCM-41$_{B(TESPIC)}$** – 534.31 eV)*. The N(1s) and C(1s) peaks were attributed to the –NCO group.

XPS spectra (Fig. 3) of **MCM-41$_{A(TESPIC-CE)}$**, **MCM-41$_{B(TESPIC)+CE}$**, and **MCM-41$_{B(TESPIC-CE)}$** show peaks for C - *C1s (**MCM-41$_{A(TESPIC-CE)}$** - 285.99 eV, **MCM-41$_{B(TESPIC)+CE}$** - 284.93 eV, **MCM-41$_{B(TESPIC-CE)}$** - 284.92 eV)*, N - *N1s (**MCM-41$_{A(TESPIC-CE)}$** - 400.91 eV, **MCM-41$_{B(TESPIC)+CE}$** - 399.21 eV, **MCM-41$_{B(TESPIC-CE)}$** - 399.42 eV)*, Si - *Si2p (**MCM-41$_{A(TESPIC-CE)}$** - 103.3 eV, **MCM-41$_{B(TESPIC)+CE}$** - 102.8 eV, **MCM-41$_{B(TESPIC-CE)}$** - 102.77 eV)*, and O - *O1s (**MCM-41$_{A(TESPIC-CE)}$** - 533.08 eV, **MCM-41$_{B(TESPIC)+CE}$** - 532.06 eV, **MCM-41$_{B(TESPIC-CE)}$** - 531.9 eV)*.

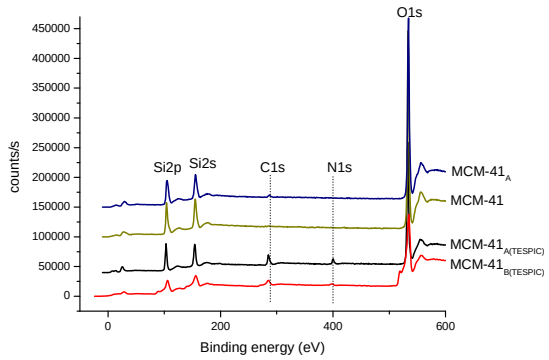

Fig. 2. XPS spectra of ***MCM-41****,* ***MCM-41$_{A}$****,* ***MCM-41$_{A(TESPIC)}$****,* ***MCM-41$_{B(TESPIC)}$***

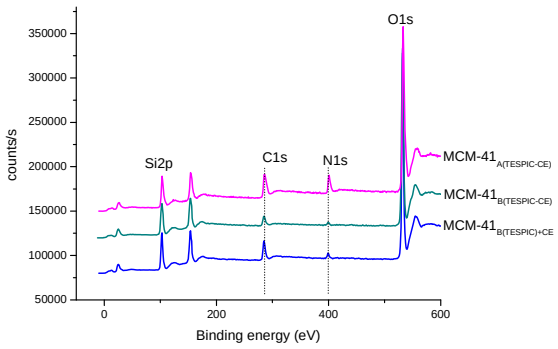

Fig. 3. XPS spectra of ***MCM-41$_{A(TESPIC-CE)}$****,* ***MCM-41$_{B(TESPIC-CE)}$****,* ***MCM-41$_{B(TESPIC)+CE}$***

In the XPS spectra of **MCM-41$_{A(TESPIC-CE)}$**, **MCM-41$_{B(TESPIC)+CE}$**, and **MCM-41$_{B(TESPIC-CE)}$**, N(1s) peaks are shifted to higher binding energy values than in the case of **MCM-41$_{A(TESPIC)}$** and **MCM-41$_{B(TESPIC)}$** and they were assigned to the nitrogen amide linkage of **TESPIC-CE**. Moreover, the XPS spectra clearly shown that regardless the methodology used for post-grafting synthesis: heterogeneous for **MCM-41$_{B(TESPIC)+CE}$** and homogeneous for **MCM-41$_{B(TESPIC-CE)}$**, the two mesoporous silicas have the same chemical composition, with the same species, **TESPIC-CE**, formed and immobilized onto silica surface.

All of these results verified that 3-(triethoxysilyl) propyl isocyanate modified crown ether (**TESPIC-CE**) was successfully immobilized on the silica surface and at the same time, in atomic content quantification based on the XPS, the atomic contents (converted in weight percents) of C and N are comparable with those found by elemental analysis (Table 1).

3.3. Thermal analysis

The conclusions drawn from the FTIR and XPS spectra may be supported also by the results of the TGA-DSC analyses shown in Figure 4 as well.

All mesoporous silica described in this work (Table 1) exhibit similar thermal behaviour with three main weight loss peaks observed from TGA-DSC curves: volatilization of the adsorbed solvent or water molecules (below 150°C), decomposition of organic fragments incorporated or grafted in the silica pores (150-550°C), and densification of the silica matrix caused by subsequent condensation reactions (above 550ºC up to 900ºC).

The first weight loss of about 1-3%wt (the lowest weight loss is 1.01%wt for **MCM-41$_{B(TESPIC)}$** and the highest weight loss is 2.66%wt for **MCM-41$_{A(TESPIC)}$**) occurs in the temperature range 30–150°C, and this process can be attributed to the loss of physically absorbed water or solvent molecules. On further heating, a weight loss with values ranging from 7.32%wt (**MCM-41$_{B(TESPIC-CE)}$**) to 24.4%wt (**MCM-41$_{A(TESPIC-CE)}$**) occurs between 150-550°C and was ascribed to the decomposition of organic fragments, TESPIC or **TESPIC-CE**, used for silica derivatization.

At higher temperature (above 550ºC up to 900ºC), the weight loss of 2.35%wt (**MCM-41$_{B(TESPIC)}$**), 3.29%wt (**MCM-41$_{B(TESPIC-CE)}$**), 2.58%wt (**MCM-41$_{B(TESPIC)+CE}$**), 3.16%wt (**MCM-41$_{A(TESPIC)}$**), and 4.76%wt (**MCM-41$_{A(TESPIC-CE)}$**) can be ascribed to the condensation of some terminal Si–OH groups on the silica surface to form Si–O–Si networks. The TGA-DSC data are consistent with the elemental analysis and XPS measurements of the mesoporous silicas samples.

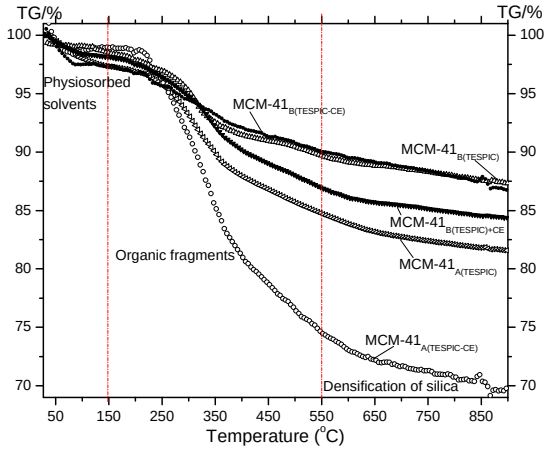

Mesoporous silicas	Δm (weight loss, %)		
t (°C)	< 150	150-550	>550
MCM-41$_{A(TESPIC)}$	2.66	12.61	3.16
MCM-41$_{A(TESPIC-CE)}$	1.01	24.40	4.76
MCM-41$_{B(TESPIC)}$	1.50	8.81	2.35
MCM-41$_{B(TESPIC)+CE}$	1.89	11.19	2.58
MCM-41$_{B(TESPIC-CE)}$	2.65	7.32	3.29

Fig. 4. TG curves of the synthesized mesoporous silicas

3.4. Powder XRD

For all synthesized silicas, the XRD patterns clearly show the hexagonal ordering of the MCM-41 structure and exhibit reflections at low diffraction angles, typically in the 2θ region: 0.6°- 6° (Fig. 5). The distinct Bragg peaks in this range are indexed as (100), (110), (200), and (210) reflections for the MCM-41 hexagonal symmetry (*p6mm* space group) [15]. The values of the corresponding unit cell parameter a_0 were calculated using formula: $a_0 = 2d_{100}/3^{½}$ where d_{100} represented the d-spacing value of the (100) diffraction peak in XRD patterns of the samples (Fig. 5).

Compared with the XRD pattern of the commercially available MCM-41 used as reference (d_{100} = 3.91 nm, d_{110}=2.25 nm, d_{200}=1.96 nm, d_{210}=1.46 nm, a_0=4.51 nm) the d_{100} spacing values of **MCM-41$_{B(TESPIC)}$** (d_{100} = 3.77 nm), **MCM-41$_{B(TESPIC-CE)}$** (d_{100} = 3.88 nm), **MCM-41$_{B(TESPIC)+CE}$** (d_{100} = 3.94 nm) are very similar, indicating that both the hexagonal ordering and the mesoporous framework of MCM-41 have been fully preserved after the grafting of the organic moieties.

On the other hand, XRD patterns of **MCM-41$_{A(TESPIC)}$** and **MCM-41$_{A(TESPIC-CE)}$** (Fig. 5) are characterised by a decreasing in 2θ (100) diffraction intensity and by the disappearance of the (110), (200), and (210) reflections, both features being indicative for the incorporation of organic moieties (TESPIC or **TESPIC-CE**) into the pore channels of the MCM-41 material, without the collapse of the pore structure.

3.5. High-resolution transmission electron microscopy (HRTEM)

In addition to XRD patterns, HRTEM micrographs (Fig. 6) further confirm the hexagonal ordering of the mesopores in **MCM-41$_{B(TESPIC-CE)}$**, **MCM-41$_{B(TESPIC)+CE}$**, and **MCM-41$_{A(TESPIC-CE)}$**.

MCM-41$_{B(TESPIC-CE)}$ and **MCM-41$_{B(TESPIC)+CE}$** clearly exhibit highly ordered mesoporous structure with d_{100} spacing values estimated at 3.6 and 3.8 nm (Fig. 6) in good agreement with the value determined from the corresponding XRD data (see Fig. 5). Hence, TEM/HRTEM micrographs confirmed that both materials have typical MCM-41 structure and that MCM-41 functionalization did not affect the hexagonal structure of MCM-41.

TEM/HRTEM image of **MCM-41$_{A(TESPIC-CE)}$** reflects the reduction of mesoscopic order with the increase of organic content (shows uniform wormlike channels distributed homogeneously throughout the bulk phase) and the unit cell parameter has been estimated at 5.26 nm (Fig. 6).

The **MCM-41$_{A(TESPIC-CE)}$** unit cell parameter, a= 5.26 nm, consistent with the value calculated from XRD data (see Fig. 5), is larger than that of **MCM-41$_{B(TESPIC-CE)}$** or **MCM-41$_{B(TESPIC)+CE}$** and this expansion is related to the greater amount of organic moiety incorporated into mesoporous matrix through co-condensation (~13%wt C) than by grafting strategies (**MCM-41$_{B(TESPIC-CE)}$** ~6%wt C and **MCM-41$_{B(TESPIC)+CE}$** ~8%wt C).

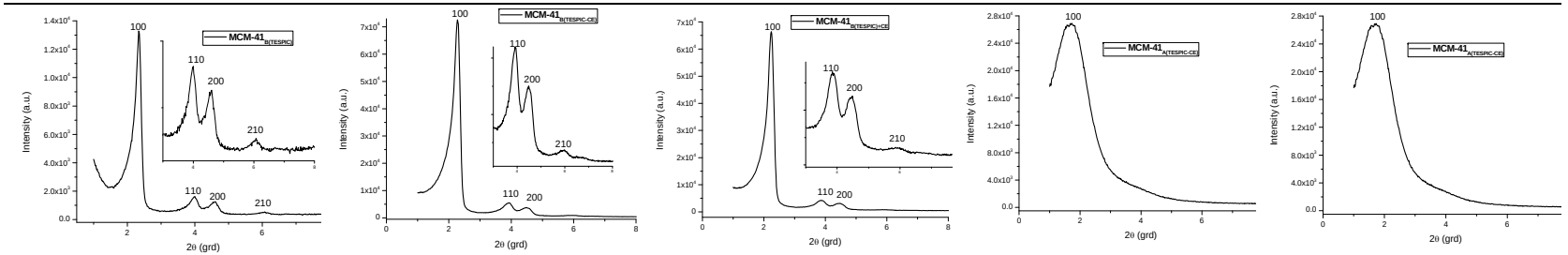

Miller indices			**MCM-41$_{B(TESPIC)}$** a =4.36 nm		**MCM-41$_{B(TESPIC-CE)}$** a = 4.48 nm		**MCM-41$_{B(TESPIC)+CE}$** a = 4.56 nm		**MCM-41$_{A(TESPIC)}$** a = 4.6 nm		**MCM-41$_{A(TESPIC-CE)}$** a = 5.15 nm	
h	k	l	2θ	d_{hkl} (nm)	2θ	d_{hkl} (nm)	2θ	d_{hkl} (nm)	2θ	d_{hkl} (nm)	2θ	d_{hkl} (nm)
1	0	0	2.33	3.77	2.27	3.88	2.23	3.94	2.21	3.98	1.98	4.46
1	1	0	3.98	2.21	3.92	2.25	3.86	2.28	-	-	-	-
2	0	0	4.58	1.92	4.48	1.97	4.45	1.98	-	-	-	-
2	1	0	6.04	1.46	5.93	1.48	5.89	1.49	-	-	-	-

Fig. 5. XRD patterns for the synthesized mesoporous silicas. Inset graphs: enlargement of the XRD pattern with diffraction planes indices.

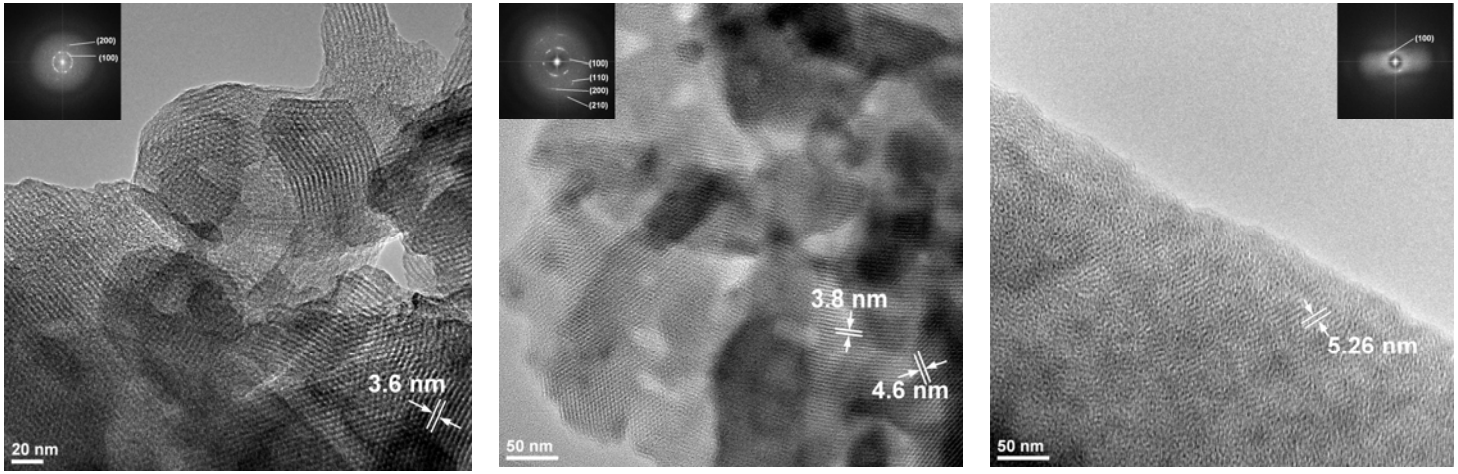

MCM-41$_{B(TESPIC-CE)}$ **MCM-41$_{B(TESPIC)+CE}$** **MCM-41$_{A(TESPIC-CE)}$**

Fig. 6. TEM images for synthesized mesoporous silicas.

3.6. Nitrogen adsorption–desorption isotherms

Using Brunauer–Emmett–Teller (BET) and Barrett–Joyner–Halenda (BJH) methods, the specific area and the pore diameter have been calculated. The structure data of **MCM-41$_{B(TESPIC-CE)}$**, **MCM-41$_{B(TESPIC)+CE}$**, and **MCM-41$_{A(TESPIC-CE)}$** mesoporous silicas (BET surface area, pore size) were summarized in Table 2.

All three materials show adsorption isotherms of type IV with H_1-type hysteresis loops at high relative pressures according to the IUPAC classification [16-19], characteristic of mesoporous materials (Fig. 7).

For **MCM-41$_{B(TESPIC-CE)}$** and **MCM-41$_{B(TESPIC)+CE}$**, the isotherms were very similar and exhibited complementary textural mesoporous frameworks and uniform pore channels, as indicated by the presence of the sharp step of capillary condensation in mesopores in the p/p^0 = 0.3–0.35 region. Grafting of **TESPIC-CE** onto silica inner surface, either by homogeneous or heterogeneous method, resulted in the reduction of surface area from ~1000 m^2/g of the pure MCM-41 used as reference to 707 m^2/g for **MCM-41$_{B(TESPIC-CE)}$** and to 903 m^2/g for **MCM-41$_{B(TESPIC)+CE}$**, suggesting that for comparable **TESPIC-CE** content into silica framework, the heterogeneous method lead to better sorption properties: higher surface area and more efficiently grafting of crown ether inside pores.

Interestingly, the **MCM-41$_{A(TESPIC-CE)}$** silica obtained by template-directed co-condensation reaction exhibits a relatively high surface area (618 m^2/g) while containing about twice as much organic content into mesoporous framework than **MCM-41$_{B(TESPIC-CE)}$** or **MCM-41$_{B(TESPIC)+CE}$**. Additionally to this feature, it is worth noting for **MCM-41$_{A(TESPIC-CE)}$** the moderate pore size increase (2.99 nm) accompanied by a large increase of the pore wall thickness (2.15 nm).

For all three mesoporous silicas the results are well consistent with the XRD and TEM/HRTEM data.

*Table 2. Textural parameters of **MCM-41$_{B(TESPIC-CE)}$**, **MCM-41$_{B(TESPIC)+CE}$**, and **MCM-41$_{A(TESPIC-CE)}$** mesoporous silicas.*

Sample	d_{100} (nm)		a_0 (nm)	S_{BET} (m^2/g)	S_{BJH} (m^2/g)	d_{pore} (nm)	t_w (nm)
	XRD	TEM					
MCM-41$_{B(TESPIC-CE)}$	3.88	3.6	4.48	707	771	2.81	1.67
MCM-41$_{B(TESPIC)+CE}$	3.94	3.8	4.56	903	846	2.66	1.89
MCM-41$_{A(TESPIC-CE)}$	4.46	4.5	5.15	618	591	2.99	2.15

S_{BET} the BET surface area, S_{BJH} adsorption cumulative surface area of pores, d_{pore} the average pore diameter calculate using BJH method, and t_w the wall thickness, calculated by a_0-d_{pore}

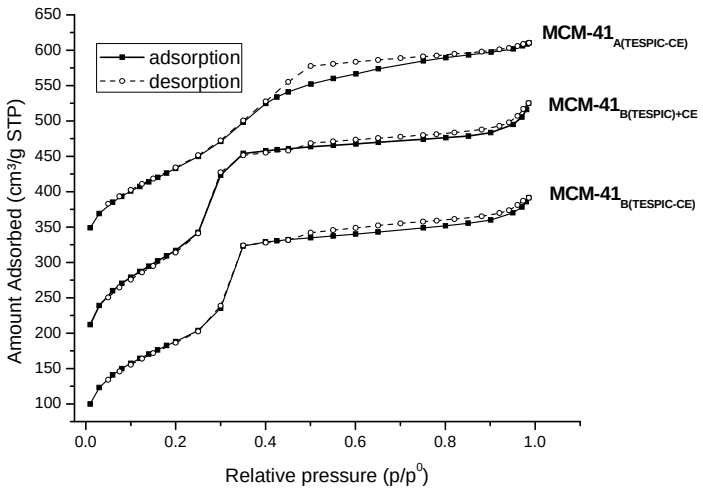

Fig. 7. Nitrogen adsorption–desorption isotherms of: ***MCM-41$_{B(TESPIC-CE)}$, MCM-41$_{B(TESPIC)+CE}$,*** *and* ***MCM-41$_{A(TESPIC-CE)}$****; the isotherms for* ***MCM-41$_{B(TESPIC)+CE}$*** *and* ***MCM-41$_{A(TESPIC-CE)}$*** *were shifted by 100 and 270 y-units, respectively.*

4. Conclusions

Novel ureido-4'-aminobenzo-15-crown-5-ether periodic mesoporous silicas have been prepared by using both template-directed co-condensation and homogeneous or heterogeneous post-synthetic grafting methodologies. Better sorption properties, in terms of surface area and content of crown ether grafted inside pores, have been observed when the post-synthetic grafting is carried out in the two-step, heterogeneous method.

Despite the lower degree of mesoorder in **MCM-41$_{A(TESPIC-CE)}$**, the silica obtained by template-directed co-condensation reaction, the relatively high surface area (618 m^2/g) for a higher content of ureido benzo-crown ether into mesoporous framework and the moderate pore size increase (2.99 nm) accompanied by a large increase of the pore wall thickness (2.15 nm), could be considered as arguments for approaching this methodology for tailoring the surface properties of mesoporous silica by organic functionalization.

Acknowledgements

Authors recognize financial support from the European Social Fund through POSDRU/89/1.5/S/54785 project: Postdoctoral Program for Advanced Research in the field of nanomaterials.

References

[1] K. Ariga, A. Vinu, J. P. Hill, T. Mori, Coord. Chem. Rev. **251**, 2562 (2007).
[2] P.K. Jal, S. Patel, B.K. Mishra, Talanta **62**, 1005 (2004).
[3] a) M.L. Bruening, D.M. Mitchell, J.S. Bradshaw, R.M. Izatt, R.L.Bruening, Anal. Chem. **63**, 21 (1991), b) J.S. Bradshaw, R.L. Bruening, K.E. Krakowiak, B.J. Tarbet, M.L.Bruening, R.M. Izatt, J.J. Christensen, J. Chem. Soc., Chem. Commun. **12**, 812 (1988).
[4] M. Barboiu, S. Cerneaux, A. Van der Lee, G. Vaughan, J. Am. Chem. Soc. **126**, 3545 (2004).
[5] A. Cazacu, Y.-M. Legrand, A. Pasc, G. Nasr, A. van der Lee, E. Mahon, M. Barboiu, PNAS **106**(20), 8117 (2009).

[6] M. Barboiu, A. Cazacu, S. Mihai, Y.-M. Legrand, G. Nasr, Y. Le Duc, E. Petit, A. Van der Lee, Microporous Mesoporous Mater. **140**, 51 (2011).
[7] S. Yajima, T. Nakajima, M. Higashi, K. Kimura, Chem. Commun. **46**, 1914 (2010).
[8] T. Matsuoka, S. Yamamoto, O. Moriya, M. Kashio, T. Sugizaki, Polym. J. **42**, 313 (2010).
[9] S. Mihai, A. Cazacu, C. Arnal-Herault, G. Nasr, A. Meffre, A. van der Lee, M. Barboiu, New J. Chem. **33**, 2335 (2009).
[10] M. Kawamura, K. Sato, Chem. Commun. 3404 (2007).
[11] A. C. Nechifor, M. G. Stoian, S. I. Voicu, G. Nechifor, Optoelectron. Adv. Mat. **4**(8) , 1118 (2010).
[12] S. Cerneaux, N. Hovnanian, J. Membr. Sci. **247**, 87 (2005).
[13] Y. Barre, M. Simon, R. Neige, R. Duval, WO03062250A1 (2003).
[14] V. S.-Yi Lin, C.-Yu Lai, S. Jeftinija, D. M. Jeftinija US2009/0252811 (2009).
[15] V. Meynen, P. Cool, E.F. Vansant, Microporous Mesoporous Mater. **125**, 170 (2009).
[16] D.H. Everett, Pure. Appl. Chem. **31**, 577 (1972).
[17] K.S.W. Sing, D.H. Everett, R.A.W. Haul, L. Moscow, R.A. Pierotti, J. Rouquerol, T. Siemieniewska, Pure Appl. Chem. **57**, 603 (1985).
[18] M.H. Lim, A. Stein, Chem. Mater. **11**, 328 (1999).
[19] W.H. Zhang, X.B. Lu, J.H. Xiu, Z.L. Hua, L.X. Zhang, M. Robertson, J.L. Shi, D.S. Yan, J.D. Holmes, Adv. Funct. Mater. **14**, 544 (2004).